Supporting Information for

Aircraft Measurements of Single Particle Size and Composition Reveal Aerosol Size and Mixing State Dictate their Activation into Cloud Droplets

G. Saliba,[a, †] D. M. Bell,[a, ‡], K. J. Suski,[a, §] J. Fast,[a] D. Imre,[b] G. Kulkarni,[a] F. Mei,[a] J. H. Mülmenstädt,[a] M. Pekour,[a] J. E. Shilling,[a] J. Tomlinson,[a] A. C. Varble,[a] J. Wang,[c] J. A. Thornton,[d] A. Zelenyuk*[a]

[a]Pacific Northwest National Laboratory, Richland, WA, USA, [b]Imre Consulting, Richland, WA, USA, [c]Washington University in Saint Louis, Saint Louis, MO, USA, [d]University of Washington, Seattle, WA, USA

[*]Corresponding author: Alla Zelenyuk (alla.zelenyuk-imre@pnnl.gov)

[†]Now at the California Air Resources Board, Sacramento, CA

[‡]Now at the Paul Scherrer Institute, Villigen, Switzerland

[§]Now at Juul Labs, San Francisco, CA

Contents of this file:

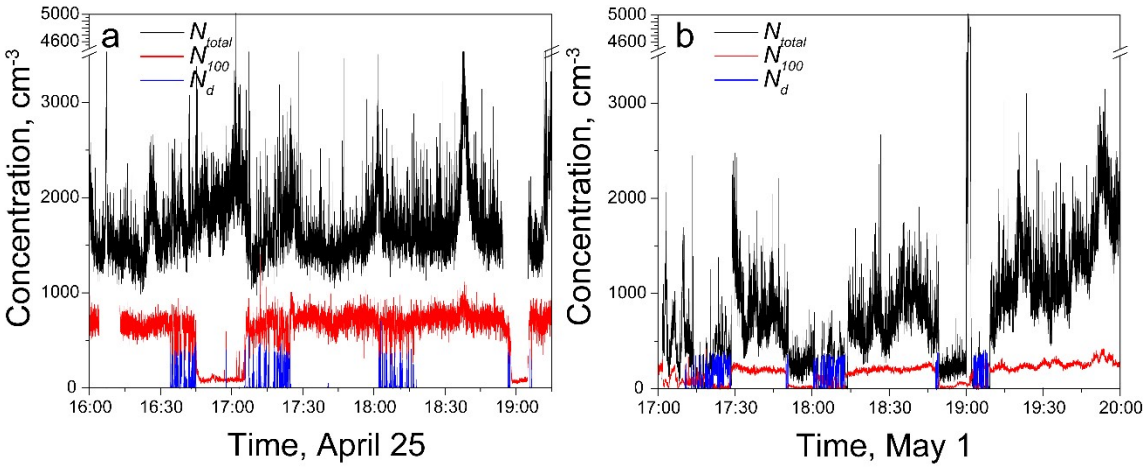

Figure S1. Temporal evolution of for total number concentrations (black line, measured by the FIMS), N100 number concentrations (red line, measured by the PCASP on April 25 and UHSAS on May 1), and droplet concentrations (blue line, measured by the FCDP).

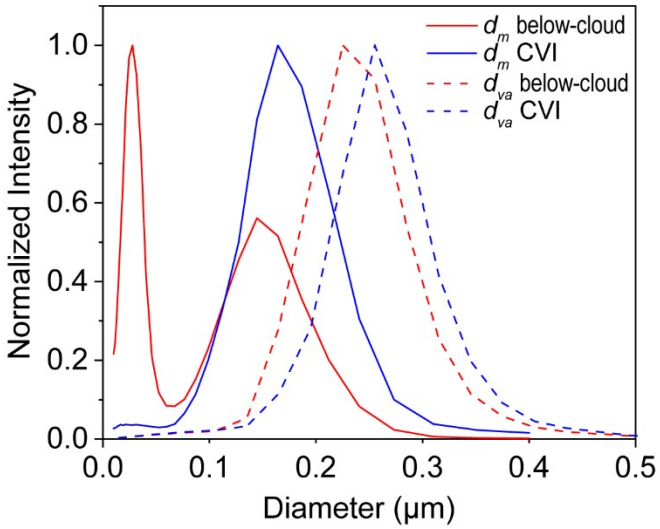

Figure S2. Flight average normalized mobility diameter (d_m, FIMS, solid lines) and vacuum aerodynamic diameter (d_{va}, miniSPLAT, dashed lines) number size distributions for below-cloud aerosol (red) and cloud droplet residuals (blue lines) sampled during the May 1 flight.

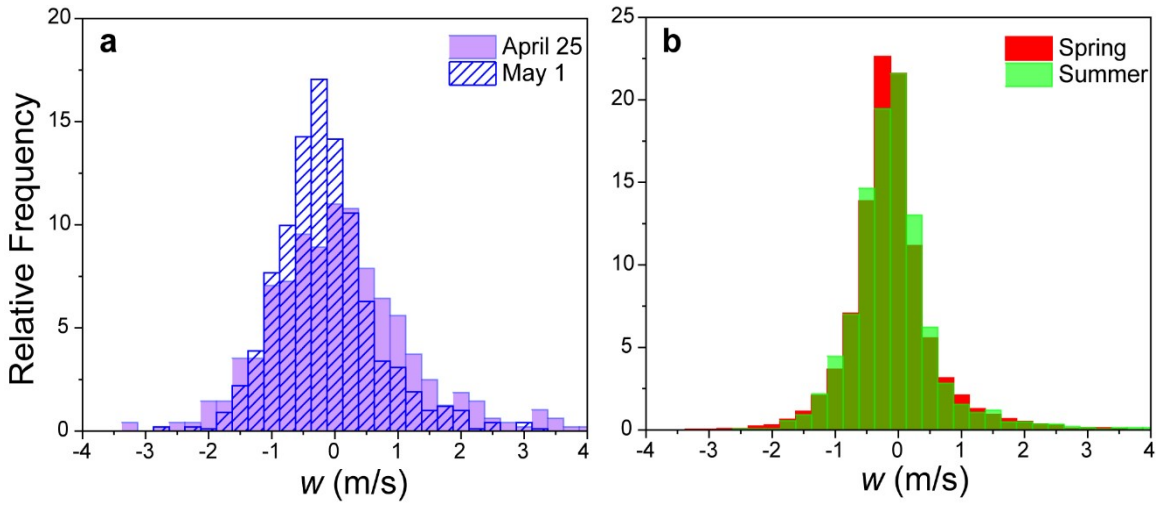

Figure S3. PDF distributions for updraft velocity (w) measured inside the clouds during **(a)** April 25 (purple) and May 1 (patterned blue) and **(b)** spring (red) and summer (green) campaigns.

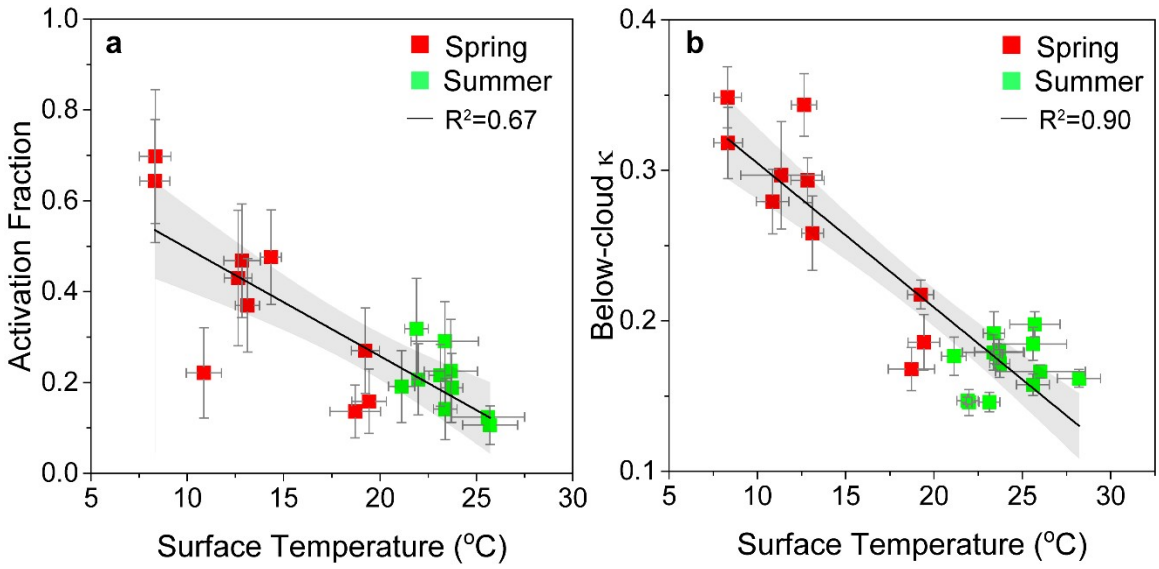

Figure S4. Correlation between **(a)** surface temperatures and activation fraction and **(b)** surface temperatures and below-cloud hygroscopicity. Red and green datapoints are for the spring and summer campaigns, respectively. The solid lines are the lines of best fit.

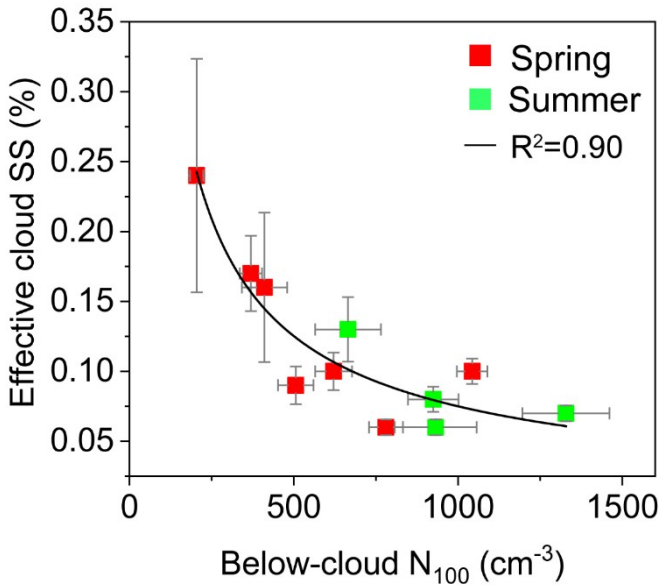

Figure S5. Effective cloud supersaturation (retrieved using methodology shown in Figure S6 based on the measured real-world mixtures) versus below-cloud accumulation-mode number concentrations (N_{100}). Red and green datapoints are for the spring and summer campaigns, respectively.

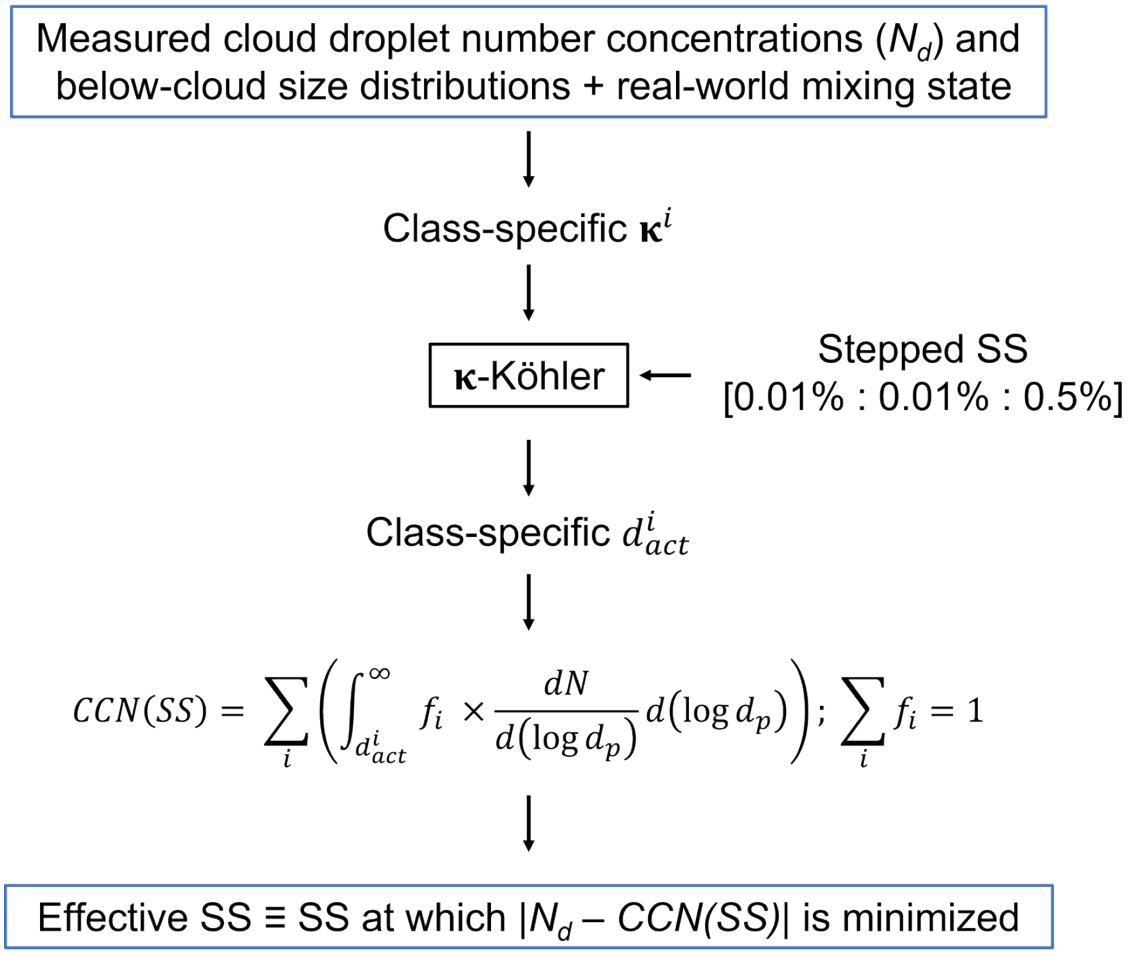

Figure S6. Methodology followed to calculate the effective cloud supersaturation using flight averages for below-cloud aerosol hygroscopicity, below-cloud particle number size distributions, and cloud droplet number concentrations (N_d). For simplicity, the same below-cloud particle number size distributions were used for all particle types. **κ**-Köhler theory calculations were performed assuming: T=288.15K, R=8.315 J.K^{-1} mol^{-1}, ρ_w=997.1 kg m^{-3}, M_w=0.018015 kg mol^{-1}, and σ_w=0.072 J m^{-2}.